LBL-11815 c.2
Preprint

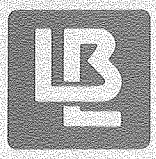

Lawrence Berkeley Laboratory
UNIVERSITY OF CALIFORNIA

Materials & Molecular Research Division

Submitted to Nuclear Science and Engineering

MIGRATION OF GAS-LIQUID INCLUSIONS IN KCℓ AND NaCℓ SINGLE CRYSTALS

Donald R. Olander, Albert J. Machiels, and Eugen Muchowski

August 1980

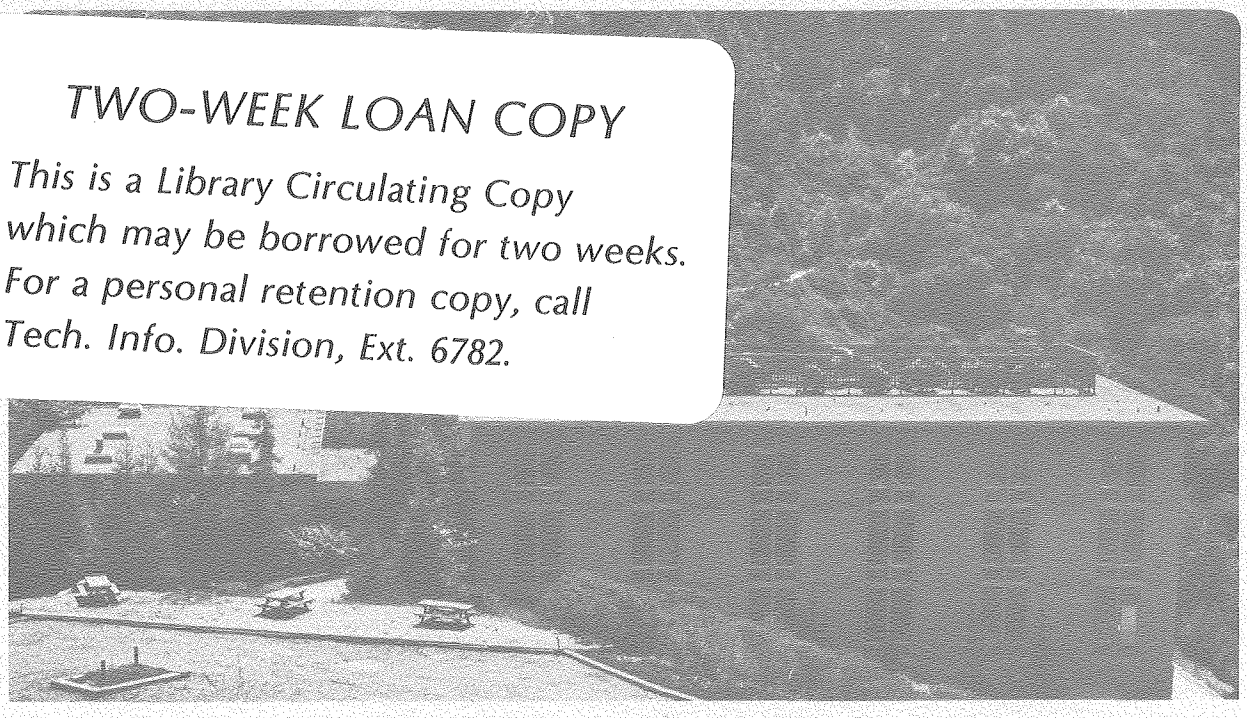

Prepared for the U.S. Department of Energy under Contract W-7405-ENG-48

DISCLAIMER

LBL-11815

MIGRATION OF GAS-LIQUID INCLUSIONS IN KCℓ AND NaCℓ SINGLE CRYSTALS

by

Donald R. Olander,

Materials and Molecular Research Division of the Lawrence Berkeley Laboratory, and
Department of Nuclear Engineering, University of California, Berkeley, California 94720, U.S.A.

Albert J. Machiels

Nuclear Engineering Program
University of Illinois, Urbana, Illinois 61801, U.S.A.

Eugen Muchowski

Institute fur Thermische Verfahrenstechnik
Universitat Karlsruhe, Federal Republic of Germany

ABSTRACT

Natural salt deposits contain small brine inclusions which can be set into motion by a temperature gradient arising from storage of nuclear wastes in the salt. Inclusions totally filled with liquid move up the temperature gradient, but cavities which are filled partly with liquid and partly by an insoluble gas move in the opposite direction. The velocities of these gas-liquid inclusions are calculated from a model which includes: heat transport in the gas/liquid/solid composite medium; vapor transport of water in the gas bubble as the principal mechanism causing cavity motion; and the effect of molecular and thermal diffusion on transport of salt in the liquid phase. An analytical expression for the inclusion velocity is obtainable with certain simplifications, which include: approximating the cubical cavity in the solid as a spherical hole containing a central gas bubble and an annular shell of liquid; neglecting interface kinetics (i.e., slow dissolution and crystallization steps) and assuming the process to be diffusion-controlled and disregarding fluid motion generated by surface tension gradients at the gas/liquid interface. The theory predicts a change in the migration direction at a critical volume fraction gas in the cavity. For gas fractions greater than this critical value, the theory gives the velocities of migration down the temperature gradient which are in satisfactory agreement with available experimental data.

A. INTRODUCTION

Natural salt deposits contain small cubical inclusions of brine distributed through the salt.[1] Temperature gradients resulting from storage of heat-generating wastes can cause the inclusions to move through the salt.[2] [3] Prediction of the rate and amount of brine-inclusion migration is necessary for the evaluation of bedded or domed salts as possible media for waste repositories.[4] [5]

Inclusions filled exclusively with liquid migrate up the temperature gradient towards the heat source. However, some inclusions also contain a gas phase consisting of water vapor and an inert gas. These two-phase inclusions usually migrate down the temperature gradient away from the heat source, remaining more-or-less cubical as they do so. A two-phase inclusion also forms when an all-liquid inclusion reaches the waste package; upon opening up at the salt-package interface, the brine partially evaporates and the inclusion reseals with some insoluble gas trapped inside. These gas-liquid inclusions proceed to move down the temperature gradient, in the opposite sense of the all-liquid inclusions. The behavior of gas-liquid inclusions in a thermal gradient is particularly relevant to the technology of nuclear waste disposal because the phenomenon provides a pathway by which radionuclides leached from the wasteform by the brine can be transported away from the waste package and thus have greater access to the biosphere.

The mechanism of thermal gradient migration of gas-liquid inclusions is shown in Fig. 1. Water vapor evaporates from the hot side of the gas bubble in the brine and is transported to the cold side where it condenses. The condensed water is recycled to the hot side by backflow of the brine,

which provides the mechanism for moving salt from the cold face of the inclusion to the hot face. The inclusion moves in the opposite direction from the salt flow.

The object of the analysis is to determine the velocity of the two-phase fluid inclusion in the thermal gradient imposed on the solid salt. We present a more detailed theory of this process than that offered by Anthony and Cline[6]. In particular, we allow for:

i) non-uniform flow field in the liquid;

ii) the effect of the heat of vaporization of water on the temperature distributions;

iii) non-uniform concentration distribution of the salt dissolved in the liquid phase.

Detailed fluid flow, heat and mass transport calculations cannot be done analytically for the actual geometry of the inclusion, which is a gas bubble in a cubical brine cavity in an infinite medium of solid. Therefore, the cubical shape of the cavity is approximated by a sphere of radius b with a central spherical bubble of radius a. The spherical shell between the gas bubble and the solid is filled with liquid. This composite sphere is embedded in an infinite medium of solid which supports a temperature gradient ∇T_∞ at large distances from the inclusion.

The calculated temperature distribution in a single-phase spherical inclusion embedded in an infinite solid[7] shows that the temperature gradient inside the sphere is uniform across the cross section. Thus, the vapor flux which is driven by the temperature gradient inside the sphere (via the temperature dependence of the vapor pressure) is also uniform over the sphere cross section. We assume that the one-dimensional nature of the vapor flux

across the central bubble is also applicable to the two-phase inclusion, which can be justified at the completion of the calculation. We define j as the flux of water vapor (mole/cm^2-sec) across the gas bubble (hot-to-cold).

In Section B, the flow field in the liquid shell needed to return the water flux arriving from the vapor phase is determined. In Section C, the temperature distributions in the gas, liquid, and solid phases are calculated. In Section D, the concentration distribution of salt dissolved in the liquid shell is determined. The water flux is calculated in Section E and in Section F, the velocity of the inclusion is computed. The theory is compared with data from the literature in Section G.

B. FLUID FLOW IN THE LIQUID SHELL

The flow of water in the liquid phase which returns the water vapor flux j requires a pressure drop in the liquid. The pressure drop is denoted by Δp_ℓ and represents the liquid pressure on the cold side of the inclusion minus that on the hot side. Δp_ℓ is determined by the quantity of fluid which is moved (which is proportional to the vapor flux j) and by the flow resistance in the liquid shell. The pressure drop must be estimated in order to determine whether it is sufficiently large to affect the vapor flux j. The connection between Δp_ℓ and j arises from the relation between pressure in a liquid and the curvature of the gas-liquid interface. The latter in turn affects the vapor pressure of water, which is the driving force for the vapor flux j.

Rather than deal with the complexity of laminar flow in a spherical liquid shell with a continuous distribution of mass flux on its inner boundary, we estimate Δp_ℓ by using the Hagen-Poiseuille formula for flow in

a straight duct:

$$\Delta p_\ell = 32 \mu_\ell \frac{L}{d_h^2} \bar{u} \tag{1}$$

where μ_ℓ is the viscosity of the liquid, L and d_h are the channel length and hydraulic diameter, respectively, and $\bar{u}$ is the mean speed of the flowing liquid. In applying Eq. (1) to the liquid shell of the spherical inclusion the flow path is considered to run from the cold side of the inclusion to the hot side around half of the circumference through the middle of the liquid shell, or

$$L \simeq \pi \frac{b + a}{2} \tag{2}$$

The hydraulic diameter is defined as 4 times the cross sectional area for flow divided by the wetted perimeter. For the liquid shell, the flow area is $\pi(b^2-a^2)$ and the wetted perimeter is $2\pi b$ (the inner boundary of the shell does not contribute to the wetted perimeter because it offers no frictional resistance to the flow). Therefore, the hydraulic diameter is:

$$d_h \simeq \frac{4 \pi (b^2-a^2)}{2 \pi b} = \frac{2 (b+a) (b-a)}{b} \tag{3}$$

The maximum backflow through the liquid shell occurs at the midplane where the average velocity is:

$$\bar{u} = \frac{1}{\rho_\ell} \frac{j(\pi a^2)}{\pi(b^2-a^2)} = \frac{j}{\rho_\ell} \frac{a^2}{(b+a) (b-a)} \tag{4}$$

where ρ_ℓ is the density of the liquid.

Substituting Eqs. (2) - (4) into Eq. (1) yields:

$$\Delta p_\ell \simeq \frac{4 \pi \mu_\ell j}{\rho_\ell a} \frac{H^2}{(H+1)^2 (H-1)^3} \tag{5}$$

where H = b/a. It is to be noted that Δp_ℓ increases very rapidly as the liquid shell becomes thin (i.e., as $H \to 1$). An idea of the magnitude of Δp_ℓ can be obtained by using physical property data for NaCl brine at $\sim 50^{\circ}C$, assuming a 10 μm diameter inclusion containing 35% by volume of gas, and taking $j = 2 \times 10^{-7}$ moles/cm^2-sec. (This value of j is computed in Section E but we borrow it for the purpose of this calculation). Using these figures, Eq. (5) gives $\Delta p_\ell \simeq 2 \times 10^{-4}$ Pa (2×10^{-9} atm). Thus, only an exceedingly small pressure drop is needed to drive the water backflow.

Because of the curvature of the bubble surface, the pressure in the liquid is smaller than the pressure of the gas, which is uniform throughout the gas bubble. The difference of the liquid pressures at the hot and cold sides of the bubble is related to the radii of curvature of the interfaces at these two locations by:

$$\Delta p_\ell = 2\gamma\left(\frac{1}{R_h} - \frac{1}{R_c}\right) \tag{6}$$

where γ is the surface tension of water and R_h and R_c are the radii of curvature on the hot and cold sides of the bubble, respectively. Thus, the bubble must depart slightly from spherical shape in order to provide the pressure driving force Δp_ℓ to return the flux of vapor crossing the bubble in the gas phase.

The vapor pressure over a curved liquid surface is different from that over a flat surface. This phenomenon is described by Kelvin's equation[8]:

$$\frac{p_w(R)}{p_w} = \exp\left[-\left(\frac{2\gamma}{RT\rho_\ell}\right)\frac{1}{R}\right] \simeq 1 - \left(\frac{2\gamma}{RT\rho_\ell}\right)\frac{1}{R} \tag{7}$$

where $p_w(\mathcal{R})$ is the vapor pressure above a surface with radius of curvature $\mathcal{R}$ and R is the gas constant. Ignoring for the moment the effect of temperature (and salt concentration) on p_w, the vapor pressure difference due only to bubble distortion is, from Eq. (7):

$$\frac{p_w(\mathcal{R}_c) - p_w(\mathcal{R}_h)}{p_w} = \left(\frac{2\gamma}{RT\rho_\ell}\right)\left(\frac{1}{\mathcal{R}_h} - \frac{1}{\mathcal{R}_c}\right) \tag{8}$$

Eliminating the difference in the reciprocal radii of curvatures between Eqs. (6) and (8) yields:

$$\left[\frac{(p_w)_{cold} - (p_w)_{hot}}{p_w}\right]_{\substack{\text{bubble}\\ \text{distortion}}} = \frac{\Delta p_\ell}{RT\rho_\ell} \tag{9}$$

where $(p_w)_{cold} = p_w(\mathcal{R}_c)$ and $(p_w)_{hot} = p_w(\mathcal{R}_h)$. Using the value of Δp_ℓ estimated previously, the fractional change in water vapor pressure due to the bubble distortion needed to drive the backflow is $\sim 10^{-12}$.

This number is to be compared with the vapor pressure difference due to the temperature gradient across the bubble, which is primarily responsible for the water flux. This is:

$$\left[\frac{(p_w)_{cold} - (p_w)_{hot}}{p_w}\right]_{\substack{\text{temp.}\\ \text{gradient}}} = -\frac{1}{p_w}\left(\frac{dp_w}{dT}\right)\left(\frac{dT_g}{dz}\right) a \simeq -\frac{1}{p_w}\left(\frac{dp_w}{dT}\right) a\, \nabla T_\infty \tag{10}$$

where dp_w/dT is the variation of the vapor pressure of water with temperature. The temperature gradient across the bubble, dT_g/dz, has been approximated by the gradient in the solid far from the inclusion, ∇T_∞. Note that the vapor pressure difference due to bubble distortion is in the opposite sense as that due to the thermal gradient, and in this way the flow resistance to the liquid backflow acts to reduce the flux j. However,

using $\nabla T_\infty = 5\ ^{o}K/cm$ and $a = 5x10^{-4}$ cm, we find that the fractional difference in water vapor pressure due to the temperature gradient is $\sim 10^{-4}$, which is 8 orders of magnitude larger than that due to bubble distortion. Thus we conclude in agreement with Anthony and Cline[6] - but for a different reason - that the resistance to the backflowing liquid is so small that it has a negligible effect upon the vapor flux j.

The flow field in the liquid shell can be estimated for a prescribed vapor flux without the necessity of confronting the Navier-Stokes equations. The radial and angular components of the velocity in the shell $a \leq r \leq b$ are denoted by u_r and u_θ. It is convenient to deal with the molar flow distribution, with components J_r and J_θ which are related to the velocity components by:

$$J_r = \rho_\ell\, u_r$$
$$J_\theta = \rho_\ell\, u_\theta \qquad (11)$$

where ρ_ℓ is the total molar density of the liquid.

The flow field is computed by neglecting the presence of dissolved salt in the liquid phase (the mole fraction of salt in saturated brine is ~ 0.1) and calculating the flow of a pure water layer. In this approximation, J_r and J_θ vanish at $r = b$ because the outer boundary of the shell is assumed to be impervious.

With reference to the section of the liquid shell shown as the shaded area in Fig. 2, the supply of water to this volume element comes from the vapor flux j across the circular cross section of the central sphere which passes through points 1 and 2. Since the rear surface of the volume element

(at r = b) is impervious to water, all of the water vapor crossing the circular cross section must return as backflow through the liquid shell, which yields:

$$2\pi \sin\Theta \int_a^b r\,(-J_\Theta)\,dr = j\pi a^2 \sin^2\Theta \tag{12}$$

The radial distribution of the J_Θ flow is sketched in Fig. 2. We assume that the shape of this profile is independent of Θ but that its magnitude changes with Θ as water is condensed or evaporated at the inner boundary of the shell. Thus, we seek a solution for J_Θ in the separable form:

$$J_\Theta = k(\Theta)\ F(r) \tag{13}$$

The function F(r) is chosen to satisfy the boundary conditions

$$J_\Theta(r=b) = F(b) = 0 \tag{14}$$

and

$$\left(\frac{\partial J_\Theta}{\partial r}\right)_{r=a} = \left(\frac{dF}{dr}\right)_{r=a} = 0 \tag{15}$$

Eq. (15) is a reflection of the absence of a shear stress at the gas/liquid boundary. Surface shear generated by surface tension gradients is not considered. A function which satisfies Eqs. (14) and (15) is:

$$F(r) = -\,(b-r)\,\left[2(b-a) - (b-r)\right] \tag{16}$$

Inserting Eq. (16) into Eq. (13) and thence into Eq. (12) determines the magnitude factor $k(\Theta)$ by:

$$a^2 k(\Theta) = \frac{j \sin\Theta}{2h} \tag{17}$$

where

$$h = \frac{2}{3}(H-1)^3 + 1/4\ (H-1)^4 \tag{18}$$

and H = b/a.

Using Eqs. (16) and (17) in Eq. (13) gives:

$$J_\theta = - jF(\eta) \sin\theta \tag{19}$$

where $\eta = r/a$ and

$$F(\eta) = \tfrac{1}{2}(H-\eta)\ (H-2+\eta)/h \tag{20}$$

The flow component J_r can be calculated from Eq. (19) and the overall continuity equation:

$$\frac{1}{r^2}\frac{\partial}{\partial r}(r^2 J_r) + \frac{1}{r\sin\theta}\frac{\partial}{\partial\theta}(\sin\theta\, J_\theta) = 0 \tag{21}$$

Integrating this equation from $r = r$ to $r = b$ and noting that $J_r(r=b) = 0$, we have:

$$-a^2 J_r = \frac{1}{\sin\theta}\frac{\partial}{\partial\theta}\left[\sin\theta \int_r^b r'\ (-J_\theta)\ dr'\right] \tag{22}$$

Substituting Eq. (19) into Eq. (22) results in:

$$J_r = - j\ U(\eta) \cos\theta \tag{23}$$

where:

$$U(\eta) = \left[(\tfrac{1}{2}H^2 - \eta H)\ (H^2 - \eta^2) + \frac{2}{3}\eta\ (H^3 - \eta^3) - \tfrac{1}{4}(H^4 - \eta^4)\right]/h \tag{24}$$

C. TEMPERATURE DISTRIBUTION IN A GAS-LIQUID INCLUSION

The temperature distribution in a stationary sphere imbedded in an infinite medium of different thermal conductivity which supports a temperature gradient in the z-direction ∇T_∞ is well-known.[7] However, if the sphere moves under the influence of a mass transport process driven by the temperature gradient, additional factors affecting heat transport appear. First, the movement of the sphere introduces a convective heat transfer term in the infinite medium, so that the temperature distribution in this region is no longer a solution of Laplace's equation. This moving-medium effect is quite small because the velocity of sphere motion is generally very small and is neglected here. The second effect is related to the change of phase which occurs at the surface of the sphere to generate the mass flux which moves the sphere. This phase change, which in the present case is vaporization of water, entails an enthalpy change which must appear in the heat transfer analysis. Finally, since the inclusion consists of a liquid containing a bubble of gas the temperature distributions must be determined by solution of the heat conduction equations in the composite medium consisting of a central sphere of gas of radius a, a shell of liquid of outer radius b surrounding the central bubble, and an external infinite medium of solid. Vaporization of the liquid from the hot portions of the surface of the bubble and condensation on the cold parts of the surface generates a mass flux j in the negative z-direction within the bubble.

In order to calculate the temperature distribution in this three-phase system, Laplace's equation must be solved for each phase and the solutions joined by appropriate conditions at a and b.

Temperature Distribution in the Solid

The general solution of Laplace's equation for the axisymmetric

spherical coordinate system is[9]:

$$T_s = \sum_{n=0}^{\infty} \left(a_n \eta^n + b_n / \eta^{n+1} \right) P_n(\mu) \tag{25}$$

where T_s is the temperature in the solid at $\eta = r/a$ and $\mu = \cos\theta$, and P_n are the Legendre polynomials. The boundary conditions at large distances from the inclusion are:

$$\frac{\partial T_s}{\partial z} \to \nabla T_\infty \text{ for } r >> a$$

$$\frac{\partial T_s}{\partial x} = \frac{\partial T_s}{\partial y} \to 0 \text{ for } r >> a$$

where x and y represent the two rectangular coordinates perpendicular to the direction of the thermal gradient. Gradients in these directions vanish far from the inclusion.

Performing the transformation from rectangular to spherical coordinates[10], the boundary conditions are written:

$$V = \mu \left(\frac{\partial T_s}{\partial \eta} \right)_{\eta=\infty} + (1-\mu^2) \left(\frac{1}{\eta} \frac{\partial T_s}{\partial \mu} \right)_{\eta=\infty} \tag{26}$$

$$0 = \left(\frac{\partial T_s}{\partial \eta} \right)_{\eta=\infty} - \mu \left(\frac{1}{\eta} \frac{\partial T_s}{\partial \mu} \right)_{\eta=\infty} \tag{27}$$

where $V = a\nabla T_\infty$.

Application of Eqs. (26) and (27) to Eq. (25) gives:

$$a_0 = T$$

$$a_1 = V \tag{28}$$

$$a_2 = a_3 = \ldots = 0$$

where T is the temperature of the solid at the z position of the middle of the inclusion but far from the inclusion in the lateral direction.

Temperature Distribution in the Gas

Neglecting convection due to the sensible heat transported by the mass flux j, the energy equation for the central gas sphere reduces to Laplace's equation, for which the solution is:

$$T_g = \sum_{n=0}^{\infty} c_n \eta^n P_n(\mu) \qquad (29)$$

Solutions involving $1/\eta^{n+1}$ are inadmissible because they are unbounded at the center of the sphere.

Temperature Distribution in the Liquid Spherical Shell

Convective heat transfer is also neglected in the spherical shell of liquid even though the flux j down the temperature gradient in the sphere must be returned by a comparable backflow up the thermal gradient in the liquid surrounding the sphere. That the convective heat transport effect is small compared to conduction in the liquid can be demonstrated by the following argument.

The energy equation for the liquid in the spherical shell is:

$$\rho_\ell C_{p\ell} \left[u_r \frac{\partial T_\ell}{\partial r} + \frac{u_\theta}{r} \frac{\partial T_\ell}{\partial \theta} \right] = k_\ell \nabla^2 T_\ell \qquad (30)$$

where ρ_ℓ, $C_{p\ell}$, and k_ℓ are the total density, heat capacity and thermal conductivity of the liquid, respectively and ∇^2 is the Laplacian operator in axisymmetric coordinates. The fluid velocity components are related

to the molar flux components J_r and J_θ by Eq. (11), so that Eq. (30) is:

$$J_r \frac{\partial T_\ell}{\partial r} + \frac{J_\theta}{r} \frac{\partial T_\ell}{\partial \theta} = \frac{k_\ell}{C_{p\ell}} \nabla^2 T_\ell \tag{31}$$

Substituting J_θ and J_r given by Eqs. (19) and (23) into Eq. (31) and using dimensionless coordinates yields:

$$- U(\eta)\ \mu \frac{\partial T_\ell}{\partial \eta} + F(\eta)\ \frac{1-\mu^2}{\eta}\ \frac{\partial T_\ell}{\partial \mu} = \frac{1}{Pe_h}\ \nabla^2 T_\ell \tag{32}$$

where the Laplacian ∇^2 is now in terms of η while $F(\eta)$ and $U(\eta)$ are the functions defined by Eqs. (20) and (24).

The Peclet number for heat transfer, Pe_h, is the product of the Reynolds and Prandtl numbers,

$$Pe_h = \left(\frac{\rho_\ell u_i a}{\mu_\ell}\right) \frac{C_{p\ell} u_\ell}{k_\ell} \tag{33}$$

where $u_i = j/\rho_\ell$ is a characteristic system velocity, in this case equal to the liquid velocity at the bubble surface due to condensation or evaporation of water.

Using typical values of the factors in Eq. (33) for brine, the constant Pe_h is found to be $< 10^{-4}$. Since the terms on the left-hand side of Eq. (32) are of order unity, so must be the right-hand side. The only way that this can be achieved with Pe_h very small is for $\nabla^2 T_\ell$ to be approximately zero. Thus, convective heat transfer can be neglected and the energy equation in the liquid shell reduces to Laplace's equation for pure conduction. The temperature distribution is thus given by:

$$T_\ell = \sum_{n=0}^{\infty} \left(d_n \eta^n + e_n/\eta^{n+1}\right) P_n(\mu) \tag{34}$$

The coefficients b_n, c_n, d_n and e_n in the solid, liquid and gas temperature distributions are determined by the following conditions at the interfaces at $r = a$ and $r = b$.

Vapor-Liquid Interface (r=a)

The requirement of temperature continuity at the gas-liquid boundary is:

$$T_g(r=a) = T_\ell(r=a) \tag{35}$$

The energy balance at the gas-liquid interface takes the form:

$$k_\ell \left(\frac{\partial T_\ell}{\partial r}\right)_a + j \cos\Theta H_\ell = k_g \left(\frac{\partial T_g}{\partial r}\right)_a + j \cos\Theta H_g \tag{36}$$

where k_g is the thermal conductivity of the gas and H_g and H_ℓ are the specific enthalpies of the vaporizing species in the two states. The difference $H_g - H_\ell$ is the heat of vaporization ΔH_v. Eq. (36) is an energy balance normal to the surface, and $j\cos\Theta$ is the radial component of the mass flux at $r = a$.

Liquid-Solid Interface (r=b)

The temperature and heat flux are continuous at this boundary:

$$T_\ell(r=b) = T_s(r=b) \tag{37}$$

and

$$k_s\left(\frac{\partial T_s}{\partial r}\right)_b = k_\ell \left(\frac{\partial T_\ell}{\partial r}\right)_b \tag{38}$$

where k_s is the thermal conductivity of the solid.

Explicit Solutions for the Temperature Distributions

The series solutions of Eqs. (25), (29) and (34) are substituted into Eqs. (35) - (38) and the coefficients of each Legendre polynomial are equated to zero. This procedure yields:

$$b_o = e_o = 0$$

$$c_o = d_o = T$$

and

$$b_n = c_n = d_n = e_n = 0 \quad \text{for } n>1$$

$$b_1 = H^3 \left[3 \frac{f' - \gamma_{\ell s} Q/H^3}{g} - 1 \right] V \tag{39}$$

$$c_1 = \frac{9 - fQ}{g} V \tag{40}$$

$$d_1 = \frac{3(2 + \gamma_{g\ell}) + \frac{2Q}{H^3}(1 - \gamma_{\ell s})}{g} V \tag{41}$$

$$e_1 = \frac{3(1 - \gamma_{g\ell}) - Q(2 + \gamma_{\ell s})}{g} V \tag{42}$$

where:

$$f' = 2 + 1/H^3 + (1-1/H^3)\ \gamma_{g\ell} \tag{43}$$

$$f = 2\ (1-1/H^3) + (1+2/H^3)\ \gamma_{\ell s} \tag{44}$$

$$g = (2+\gamma_{g\ell})\ (2+\gamma_{\ell s}) + \frac{2}{H^3}\ (1-\gamma_{g\ell})\ (1-\gamma_{\ell s}) \tag{45}$$

$$Q = \frac{j\ \Delta H_v}{k_\ell\ VT_\infty} \tag{46}$$

$$\gamma_{g\ell} = k_g/k_\ell \tag{47}$$

$$\gamma_{\ell s} = k_\ell/k_s \tag{48}$$

The equations above combined with Eq. (28) provide a complete description of the temperature distributions, T_s, T_g and T_ℓ.

$$T_s = T + \left(V\eta + \frac{b_1}{\eta^2} \right) \mu \tag{49}$$

$$T_g = T + c_1 \eta \mu \tag{50}$$

$$T_\ell = T + \left(d_1 \eta + \frac{e_1}{\eta^2} \right) \mu \tag{51}$$

Solution for the Thermal Gradient Amplification Factor

Noting [from Eq. (50)] that $c_1 = a(dT_g/dz)$, and $V = a\nabla T_\infty$, Eq. (40) is equivalent to:

$$\frac{dT_g}{dz} = \frac{9 - fQ}{g} \nabla T_\infty \tag{52}$$

The coefficient Q is treated as follows. The bubble contains an inert gas through which water vapor diffuses in the negative z-direction. The water flux is given by[10]:

$$j = \left(\frac{D_v p_{tot}}{p_I RT}\right) \frac{dp_w}{dz} \tag{53}$$

where D_v is the diffusion coefficient of water vapor in the gas, p_{tot} is the total gas pressure, p_w is the vapor pressure of saturated brine and $p_I = p_{tot} - p_w$ is the pressure of the inert gas in the bubble. For the present analysis the effect of varying salt concentration on the vapor pressure can be neglected and Eq. (53) becomes:

$$j = \frac{D_v p_{tot}}{p_I RT} \frac{dp_w}{dT} \frac{dT_g}{dz} = S \frac{dT_g}{dz} \tag{54}$$

Substituting Eq. (54) into Eq. (46) and thence into Eq. (52) permits the thermal gradient amplification factor to be determined:

$$A \equiv \frac{1}{\nabla T_\infty} \frac{dT_g}{dz} = \frac{9}{g + \frac{f}{\gamma_{\ell s}} \left(\frac{S\Delta H_v}{k_s}\right)} \tag{55}$$

When vaporization is neglected and the liquid and solid have the same thermal conductivities ($\gamma_{\ell s} = 1$), Eq. (55) reduces to the classical result for a stationary sphere[7] :

$$A(\gamma_{\ell s}=1) = \frac{1}{\nabla T_\infty}\frac{dT_g}{dz} = \frac{3}{2 + \gamma_{g\ell}} \qquad (56)$$

The amplification factors of Eqs.(55) and (56) are compared in Fig. 3 and some of the properties for the calculations are shown in Tables 1 - 4. The volume fraction of gas in the inclusion is assumed to be 35%.. The three-phase calculation predicts a large influence of the latent heat on heat transport in the bubble. If $\gamma_{\ell s}$ in Eq. (55) were very large, the high conductivity of the liquid shell would eliminate the perturbation of the temperature distribution due to the necessity of transporting the latent heat of vaporization across the bubble. For the brine/NaCl combination, however, $\gamma_{\ell s} \approx 1/6$, and the liquid phase is a poorer conductor of heat than the solid. Thus, the "insulating blanket" of liquid around the gas sphere impedes dissipation of the heat of vaporization moved by the flux j across the bubble. In the limit as $\gamma_{\ell s} \to 0$, $dT_g/dz \to 0$ because there are no means of returning the latent heat transported across the bubble by conduction in the liquid or in the solid.

D. CONCENTRATION DISTRIBUTION OF SALT IN THE LIQUID SHELL

The flux of dissolved salt in the liquid has radial and angular components, each of which consists of a convective term and a diffusion term. These components are:

$$j_{sr} = -D_\ell \left[\frac{\partial C_s}{\partial r} - \sigma C_s \left(\frac{\rho_\ell - C_s}{\rho_\ell} \right) \left(\frac{\partial T_\ell}{\partial r} \right) \right] + \frac{J_r C_s}{\rho_\ell} \qquad (57)$$

$$j_{s\theta} = -\frac{D_\ell}{r} \left[\frac{\partial C_s}{\partial \theta} - \sigma C_s \left(\frac{\rho_\ell - C_s}{\rho_\ell} \right) \left(\frac{\partial T_\ell}{\partial \theta} \right) \right] + \frac{J_\theta C_s}{\rho_\ell} \qquad (58)$$

where the total flow components J_r and J_θ are those calculated in Section B, D_ℓ is the diffusion coefficient of salt in water, and C_s is the concentration of dissolved salt at position (r,θ) in the shell. The Soret coefficient, σ, is taken as negative when solute moves towards the cold end (which is the case for NaCl or KCl solutions). In these expressions $(\rho_\ell - C_s)/\rho_\ell$ may be approximated by unity without greatly affecting the Soret term.

The conservation equation for salt in the liquid shell is:

$$\text{div } \underline{j}_s = 0 \qquad (59)$$

Substituting Eqs. (57) and (58) into this relation results in the diffusion equation:

$$D_\ell \nabla^2 C_s = \frac{\partial C_s}{\partial r} \left[\frac{J_r}{\rho_\ell} + D_\ell \sigma \left(\frac{\partial T_\ell}{\partial r} \right) \right] + \frac{1}{r} \frac{\partial C_s}{\partial \theta} \left[\frac{J_\theta}{\rho_\ell} + \frac{D_\ell \sigma}{r} \left(\frac{\partial T_\ell}{\partial \theta} \right) \right] \qquad (60)$$

Using Eqs. (19) and (23) for J_r and J_θ, Eq. (51) to calculate $\left(\frac{\partial T_\ell}{\partial r} \right)$ and $\left(\frac{\partial T_\ell}{\partial \theta} \right)$ and casting Eq. (60) into dimensionless terms, we have:

$$\nabla^2\phi = -\left[Pe_m\, U(\eta) - \sigma\left(d_1 - \frac{2e_1}{\eta^3}\right)\right]\mu\,\frac{\partial\phi}{\partial\eta} + \left[Pe_m\, F(\eta) + \sigma\left(d_1 + \frac{e_1}{\eta^3}\right)\right]\frac{1-\mu^2}{\eta}\,\frac{\partial\phi}{\partial\mu} \tag{61}$$

where ϕ is the salt concentration relative to C_s^{sat}:

$$\phi = \frac{C_s}{C_s^{sat}} \tag{62}$$

and Pe_m is the Peclet number for mass transfer:

$$Pe_m = \left(\frac{\rho_\ell u_i a}{\mu_\ell}\right)\left(\frac{\mu_\ell}{\rho_\ell D_\ell}\right) \tag{63}$$

where

$$u_i = j/\rho_\ell \tag{64}$$

is the characteristic velocity upon which the Reynolds number is based and $\mu_\ell/\rho_\ell D_\ell$ is the Schmidt number of the liquid. Using properties of NaCl brine and a typical value of the water vapor flux j, Pe_m is found to be $< 10^{-3}$, and the Soret term in the brackets of Eq(61) are $\sim 10^{-5}$. Therefore the diffusion equation can be reduced to the Laplacian form

$$\nabla^2\phi = 0 \tag{65}$$

At the outer boundary of the liquid shell, the concentration in the liquid is assumed to be equal to the saturation concentration at the local temperature. Kinetic restrictions to dissolution of the solid salt or precipitation from the liquid phase are not considered in this analysis. Because the temperature variation around the inclusion is small, the saturation concentration may be expressed as a Taylor series about the value at the mean temperature:

$$C_s(r=b) = C_s^{sat} + \left(\frac{dC_s^{sat}}{dT}\right)\left[T_s(r=b) - T\right] \tag{66}$$

Evaluating the temperature change around the circumference of the solid-liquid interface from Eq. (25) and the coefficients derived thereafter, we have

$$T_s(r=b) = T + (VH+b_1/H^2)\,\mu \tag{67}$$

This equation is exact because the coefficients of the higher order Legendre polynomials in Eq. (25) are all zero. Substituting Eq. (67) into (66) yields:

$$C_s(r=b) = C_s^{sat} + \left(\frac{dC_s^{sat}}{dT}\right)(VH+b_1/H^2)\,\mu \tag{68}$$

In this equation, $\left(dC_s^{sat}/dT\right)$ is the change in salt solubility in water with temperature.

In dimensionless terms, Eq. (68) is:

$$\phi(\eta=H) = 1 + q\mu \tag{69}$$

where:

$$q = \frac{1}{C_s^{sat}}\left(\frac{dC_s^{sat}}{dT}\right)\left(1 + \frac{b_1}{VH^3}\right) \quad H\,a\,\nabla T_\infty \tag{70}$$

The factor q tends to drive a salt flux in the opposite sense as does the water backflow. This term is the one responsible for the movement of all-liquid inclusions up the temperature gradient. Using typical values

for NaCl brine, H = 1.4, ∇T_∞ = 5 K/cm, a = 5 μm and $b_1 Vh^3$ from Eq. (39), we find that $q \simeq 10^{-5}$.

The boundary condition at r = a which prevents flow of salt into the gas phase is

$$\left(j_{sr}\right)_{r=a} = 0 \tag{71}$$

Expressing j_{sr} by Eq. (57) and noting that $\left(j_{sr}\right)_{r=a} = j \cos\theta$, this boundary condition becomes:

$$D_\ell \left[\left(\frac{\partial C_s}{\partial r} \right)_{r=a} - \sigma C_s(r=a) \left(\frac{\partial T_\ell}{\partial r} \right)_{r=a} \right] + \frac{j\, C_s(r=a)\, \mu}{\rho_\ell} = 0 \tag{72}$$

Using the liquid temperature distribution given by Eq. (51), this boundary condition can be written in dimensionless terms as:

$$\left(\frac{\partial \phi}{\partial \eta} \right)_{\eta=1} = - \left[Pe_m - \sigma(d_1 - \hat{2} e_1) \right] \phi(\eta = 1)\, \mu = - Pe_m'\, \phi(\eta=1)\mu \tag{73}$$

where Pe_m is the Peclet number of Eq. (63). The Soret term is much smaller than the convective term.

The task at hand is to solve Eq. (65) subject to Eqs. (69) and (73). An accurate approximate method is available because q and Pe_m' are very small. In the limit that these two parameters approach zero, the solution is $\phi = 1$ (i.e., the liquid is everywhere saturated with salt at temperature T). Thus we are led to a solution which includes first order perturbations in q and Pe_m', where Pe_m' is the bracketed term in Eq. (73).

$$\phi = 1 + q\xi + Pe_m'\Omega \tag{74}$$

where ξ and Ω are functions of η and μ which are to be determined. Higher order terms (i.e., with coefficients q^2, (Pe_m'), and $q\, Pe_m'$) are neglected. Substituting Eq. (74) into Eqs. (65), (69) and (73), collecting and equating

to zero those terms with coefficients Pe_m' and q yields:

$$\nabla^2\Omega = 0 \tag{75}$$

$$\Omega(\eta=H) = 0 \tag{76}$$

$$\left(\frac{\partial\Omega}{\partial\eta}\right)_{\eta=1} = -\mu \tag{77}$$

and:

$$\nabla^2\xi = 0 \tag{78}$$

$$\xi(\eta=H) = \mu \tag{79}$$

$$\left(\frac{\partial\xi}{\partial\eta}\right)_{\eta=1} = 0 \tag{80}$$

The solution of Eq. (75) is:

$$\Omega = \sum_{n=0}^{\infty} \left(r_n\eta^n + s_n/\eta^{n+1}\right) P_n(\mu) \tag{81}$$

Substituting Eq. (81) into Eqs. (76) and (77) shows that $r_n = s_n = 0$ for $n \neq 1$ and:

$$r_1 = -\frac{1}{2H^3 + 1} \tag{82}$$

$$s_1 = \frac{H^3}{2H^3 + 1} \tag{83}$$

so that:

$$\Omega = \eta\left[\frac{(H/\eta)^3 - 1}{2H^3 + 1}\right]\mu \tag{84}$$

The general solution of Eq. (78) for ξ is of the same form as that for Ω given by Eq. (81). Using this series in Eqs. (79) and (80) gives:

$$\xi = \frac{H^2}{2H^3+1}\left(2\eta + \frac{1}{\eta^2}\right)\mu \tag{85}$$

It is to be noted that the perturbation functions ξ and Ω do not contain higher order Legendre polynomials (i.e., P_2, P_3,....).

E. WATER FLUX IN THE BUBBLE

The next step in determining the velocity of the two-phase inclusion is to calculate the water vapor flux across the bubble, j. The angular dependence of the vapor/liquid interface termperature, $T_g(\eta=1)$, and salt concentration at the surface, $\phi(\eta=1)$, contain only constant terms and terms linear in $\mu = \cos\theta$ (but no higher order Legendre polynomials). Therefore, the flux j, which depends only upon these two quantities, is constant over the entire cross section of the bubble perpendicular to the z-axis, as was initially assumed.

Since both j and the coefficient in the parentheses in Eq. (53) are constants, p_w is a linear function of z and dp_w/dz can be regarded as the difference in the vapor pressures of water at the points on the bubble surface intersected by a chord parallel to the z-axis divided by the length of the chord. Interpreting p_w as the vapor pressure of water over a brine solution of temperature T_g and salt concentration C_s allows the gradient in Eq. (53) to be written as:

$$\frac{dp_w}{dz} = \left(\frac{\partial p_w}{\partial T}\right)_{C_s}\left(\frac{dT_g}{dz}\right)_{r=a} + \left(\frac{\partial p_w}{\partial C_s}\right)_T\left(\frac{dC_s}{dz}\right)_{r=a} \tag{86}$$

It is convenient to express the effect of salt on the water vapor pressure over brine solutions by the boiling point elevation function $\Delta T(T,C_s)$, which is defined in terms of the vapor pressure of pure water p_w^o by:

$$p_w(T,C_s) = p_w^o \left[T-\Delta T(T,C_s)\right] \tag{87}$$

That is, the water pressure over a brine solution at temperature T and salt concentration C_s is equal to the vapor pressure of pure water at a temperature ΔT lower than the actual temperature T. Using Eq. (87) and neglecting the temperature dependence of ΔT (which is small), the coefficients of the temperature and concentration gradients in Eq. (86) are:

$$\left(\frac{\partial p_w}{\partial T}\right)_{C_s} = \left(\frac{dp_w^o}{dT}\right)_{T-\Delta T}\left(1 - \frac{\partial \Delta T}{\partial T}\right) \simeq \left(\frac{dp_w^o}{dT}\right)_{T-\Delta T}$$

and (88)

$$\left(\frac{\partial p_w}{\partial C_s}\right)_T = -\left(\frac{dp_w^o}{dT}\right)_{T-\Delta T}\left(\frac{\partial \Delta T}{\partial C_s}\right)$$

Inserting Eq. (88) into (86) and the result into Eq. (53) gives:

$$j = S\left[\left(\frac{dT_g}{dz}\right)_{r=a} - \left(\frac{\partial \Delta T}{\partial C_s}\right)\left(\frac{dC_s}{dz}\right)_{r=a}\right] \tag{89}$$

where:

$$S = \frac{D_v p_{tot}}{p_I RT}\left(\frac{dp_w^o}{dT}\right)_{T-\Delta T} \tag{90}$$

The brine concentration at the gas/liquid interface is, from Eqs. (62) and (74):

$$C_s(r=a) = C_s^{sat}\left[1 + q\xi(\eta=1) + Pe_m'\Omega(\eta=1)\right] \tag{91}$$

At the bubble surface, $z = a\cos\theta = a\mu$, so using Eqs. (84) and (85) for Ω and ξ, results in:

$$\left(\frac{dC_s}{dz}\right)_{r=a} = \frac{1}{a}\left(\frac{\partial C_s}{\partial \mu}\right)_{\eta=1} = \frac{C_s^{sat}}{a}\left[\left(\frac{3H^2}{2H^3+1}\right)q + \left(\frac{H^3-1}{2H^3+1}\right)Pe_m'\right] \tag{92}$$

Using Eq. (52) for the temperature gradient and Eq. (92) for the salt concentration gradient in Eq. (89) and eliminating the parameters Q, Pe_m' and q by use of Eqs.(46), (63), (70) and (73) yields an equation which can be solved for j. The result is:

$$j = \frac{9\, SVT_\infty\,(1-\varepsilon_1-\varepsilon_2)/g}{1 + \frac{Sf\Delta H_v}{gk_\ell}(1-\varepsilon_3) + \frac{SC_s^{sat}}{D_\ell\rho_\ell}\left(\frac{\partial\Delta T}{\partial C_s}\right)\left(\frac{H^3-1}{2H^3+1}\right)\left(1-\sigma\rho_\ell D_\ell\frac{h'\Delta H_v}{gk_\ell}\right)} \tag{93}$$

where f, g and S are given by Eqs. (44), (45) and (90) respectively, and

$$\varepsilon_1 = f'\left(\frac{H^3}{2H^3+1}\right)\left(\frac{\partial\Delta T}{\partial C_s}\right)\left(\frac{dC_s^{sat}}{dT}\right) \tag{94}$$

$$\varepsilon_2 = -\gamma_{g\ell}\,\sigma C_s^{sat}\left(\frac{H^3-1}{2H^3+1}\right)\left(\frac{\partial\Delta T}{\partial C_s}\right) \tag{95}$$

$$\varepsilon_3 = \frac{g\gamma_{\ell s}}{f(2H^3+1)}\left(\frac{\partial\Delta T}{\partial C_s}\right)\left(\frac{dC_s^{sat}}{dT}\right) \tag{96}$$

$$h' = 2\left(\frac{2H^3+1}{H^3} + \gamma_{\ell s}\,\frac{H^3-1}{H^3}\right) \qquad (97)$$

and f' is given by Eq. (43)

F. INCLUSION VELOCITY

The inclusion velocity is related to the salt flux crossing the midplane of the liquid shell by the mass balance over the control cylinder shown in Fig. 4. This volume moves with the inclusion at velocity v, so that solid salt enters the left-hand face at a rate $\pi b^2 \rho_s v$. Salt moves out of the control cylinder across the annulus formed by the liquid shell on the right-hand face at a rate equal to the integral of the salt flux component $(-j_{s\theta})_{\mu=0}$ over the annulus, or:

$$\int_a^b 2\pi r \left(-j_{s\theta}\right)_{\mu=0} dr$$

At steady-state, the rate of salt input over the left-hand face of the control cylinder must equal the output rate from the right-hand face, or:

$$v = \frac{2}{\rho_s b^2}\int_a^b r\,(-j_{s\theta})_{\mu=0}\,dr = \frac{2}{\rho_s H^2}\int_1^H \eta\,(-j_{s\theta})_{\mu=0}\,d\eta \qquad (98)$$

Using Eq. (58) for $j_{s\theta}$, Eq. (62) for the dimensionless concentration ϕ, expressing J_θ by Eq. (19) and calculating $(\partial T_\ell/\partial\theta)$ with the help of Eq. (51) results in:

$$\left(-j_{s\theta}\right)_{\mu=0} = \frac{D_\ell}{a\eta}\,C_s^{sat}\left[-\left(\frac{\partial\phi}{\partial\mu}\right)_{\mu=0} + \sigma\,\phi(\mu=0)\,\eta\left(d_1 + \frac{e_1}{\eta^3}\right)\right]$$

$$+ \frac{j}{\rho_\ell}\,F(\eta)\,C_s^{sat}\,\phi(\mu=0) \qquad (99)$$

The function ϕ is given by Eq. (74) wherein the perturbation functions are determined by Eqs. (84) and (85). Substituting these into Eq. (99) yields:

$$\left(-j_{s\theta}\right)_{\mu=0} = -\frac{D_\ell}{a\eta} C_s^{sat} \left[\eta \frac{(H/\eta)^3-1}{2H^3+1} Pe_m + \frac{H^2}{2H^3+1}\left(2\eta + \frac{1}{\eta 2}\right)q\right]$$

$$+ \frac{D_\ell}{a\eta} C_s^{sat} \sigma \eta \left(d_1 + \frac{e_1}{\eta^3}\right) + j\, F(\eta) \frac{C_s^{sat}}{\rho_\ell} \qquad (99)$$

Inserting this result into Eq. (98) yields the migration velocity:

$$v = \frac{D_\ell\, C_s^{sat}}{\rho_s a}\left\{\frac{3Pe_m - 2q(H^2-1/H)}{2H^3+1} + \sigma\left(d_1 - \frac{2e_1}{H^3}\right)\right\} \qquad (100)$$

q, Pe_m, d_1 and e_1 are defined by Eqs. (70), (63), (41) and (42) respectively. Noting that these parameters are proportional to $(a\nabla T_\infty)$, the above expression yields a linear dependence upon the temperature gradient but none on inclusion size.

In the limit as $H \to \infty$ (i.e., an all-liquid inclusion), Eq. (100) reduces to:

$$(v)_{H\to\infty} = -\frac{D_\ell}{\rho_s}\left[\frac{dC_s^{sat}}{dT} - \sigma C_s^{sat}\right]\frac{3}{2+\gamma_{\ell s}} \nabla T_\infty \qquad (101)$$

which is the formula derived by Anthony and Cline[11] when interface kinetics are neglected. The negative sign of v in Eq. (101) means that the all-liquid

inclusion moves up the temperature gradient. For all-liquid inclusions, it has been shown by Anthony and Cline[11] that interface kinetics is generally rate-controlling. Therefore, Eqs. (100) and (101), which are based on a diffusion-limited transport model, are expected to overestimate the velocities of migration.

In the limit as $H \to 1$, v should become zero. However, as $H \to 1$ in Eq. (100), v approaches the value $C_s^{sat} j/(\rho_s \rho_\ell)$, and j of Eq. (93) does not vanish. The reason that the model fails in this limit is that the water backflow is assumed to occur without flow resistance in the liquid shell. As the liquid shell becomes thinner, the backflow still returns the vapor flux j but at ever higher speeds. Eventually, however, the assumption of negligible frictional resistance to the backflow fails because Δp_ℓ of Eq. (5) approaches infinity as $H \to 1$. The difference in the radii of curvature of the liquid-gas interface on the hot and cold sides become significant in order to provide the pressure drop Δp_ℓ. The required distortion of the gas-liquid interfaces on the hot and cold sides becomes impossible to achieve for a very thin liquid film adhering to the inside of the solid cavity and the hot face simply dries out, leaving a puddle of liquid at the cold side. However, the exact geometry of the inclusion is a bubble in a cubical inclusion. For a volume gas fraction equal to 0.52, the bubble would be tangent to the six inner sides of the inclusion. This constitutes a significant departure from the geometry adopted in these calculations. Therefore this model is not expected

to provide a good description of the phenomena involved when $H < 1.25$ and so the failure of the model as $H \to 1$ does not appear to be practical significance.

G. COMPARISON OF THEORY AND EXPERIMENT

A compilation of the various parameters appearing in Eq. (100) has been prepared for the systems: sodium chloride-water-air and potassium chloride-water-air[13]. Using the compiled values, shown in Tables 1 - 4, the resulting migration velocities are plotted in Figs. 5 and 6 together with data obtained by Anthony and Cline[6], Wilcox[3] and Olander et al.[12]

For sodium chloride brines (Fig. 5), the theory predicts a change in direction of inclusion migration at a gas volume fraction between 0.03 and 0.06 depending on the temperature. The experimental velocities obtained in Ref. (12) (for gas volume fractions between 0.06 and 0.22) are lower than the computed values while Wilcox's data (gas volume fractions unreported) are within the range of calculated values.

For potassium chloride brines (Fig. 6), the theory predicts a change in direction of inclusion migration at a gas volume fraction equal to ~ 0.15. The experimental and theoretical values of the migration velocities are in good agreement.

In summary, by assuming a spherically symmetric system, an analytical expression for the migration velocity of a two-phase inclusion in a salt matrix has been derived. The theory predicts changes in direction of inclusion migration and velocities in the direction of decreasing temperatures in good agreement with available experimental data.

ACKNOWLEDGEMENT

This work was supported by the U.S. Department of Energy through the Office of Basic Energy Sciences and the Office of Nuclear Waste Isolation of the Battelle Columbus Laboratories, under Contract W-7405-ENG-48.

REFERENCES

1. Isherwood, D. J., "Fluid Inclusions In Salt - An Annoted Bibliography", USDOE Report UCID-18102 (January 1979).

2. Wilcox, W. R., Indust. Eng. Chem., 60, 13 (1968).

3. Wilcox, W. R., Indust. Eng. Chem., 61, 76 (1969).

4. Roedder, E., and Belkin, H. E., "Application of Studies of Fluid Inclusions in Permian Salado Salt, New Mexico, to Problems of Siting the Waste Isolation Pilot Plant", in "Scientific Basis for Nuclear Waste Management", Ed. McCarthy, G. J., Vol. 1, Plenum Press (1979).

5. Jenks, G. H., "Effects of Temperature, Temperature Gradients, Stress, and Irradiation on Migration of Brine Inclusions In a Salt Repository", USDOE Report ORNL-5526 (July 1979).

6. Anthony, T. R. and Cline, H. E., Acta Metallurgica, 20, 247 (1972).

7. Carslaw, H. S., and Jaeger, J. C., "Conduction of Heat in Solids", p. 426, 2d edition, University Press, Oxford (1959).

8. Atkins, P. W., "Physical Chemistry", p. 194, W. H. Freeman and Company, (1978).

9. Hildebrand, F. B., "Advanced Calculus for Engineers", p. 429, Prentice-Hall, Inc., (1949).

10. Bird, R. B., Stewart, W. E. and Lightfoot, C. N., "Transport Phenomena", John Wiley, (1960).

11. Anthony, T. R., and Cline, H. E., J. Appl. Phys. 42, 3380 (1971).

12. Olander, D. R., Machiels, A. J., Balooch, M., Muchowski, E., Yagnik, S. K., Trans. Amer. Nucl. Soc., 34, 352 (1980).

13. Machiels, A. J., "Migration of Two-Phase Inclusions: Compilation of Data", UCID-80 (1980).

Table 1 Properties of Saturated Aqueous Solutions[13]

Salt	Temperature ^{o}C	Solubility in Water $C_s^{sat} \times 10^2$, $\frac{mole}{cm^3}$	Liquid Density $\rho_\ell \times 10^2$, $\frac{mole}{cm^3}$	Solid Density $\rho_s \times 10^2$, $\frac{mole}{cm^3}$
NaCl	25	0.540	5.448	3.699
	50	0.545	5.378	3.687
	75	0.551	5.304	3.676
	100	0.560	5.228	3.664
	125	0.569	5.138	3.653
	150	0.580	5.041	3.640
	175	0.594	4.937	3.628
	200	0.609	4.830	3.615
	225	0.627	4.720	3.601
	250	0.648	4.611	3.587
KCl	40	0.454	5.165	2.66

Table 2 Parameters for Calculating the Mass Transfer Factor, S [Eq. (90)] (13)

Salt	Temperature ^{o}C	Water Diffusivity In Air $D_v P_{tot}$, $\frac{bar\text{-}cm^2}{sec}$	Boiling Point Elevation ΔT, ^{o}C	Water Vapor Pressure $\left(p_w^o\right)_{T-\Delta T}$, bar	Inert Gas Pressure p_I, bar	$\left(\frac{dp_w^o}{dT}\right)_{T-\Delta T}$ $\frac{bar}{K}$	Mass Transfer Factor $Sx10^7$, $\frac{mole}{sec\text{-}cm\text{-}K}$
NaCl	25	0.262	4.76	0.024	1.01	0.0015	0.15
	50	0.303	5.71	0.092	1.09	0.0048	0.49
	75	0.347	6.82	0.288	1.18	0.013	1.28
	100	0.393	8.09	0.753	1.26	0.028	2.84
	125	0.442	9.55	1.716	1.35	0.056	5.54
	150	0.493	11.22	3.491	1.43	0.099	9.75
	175	0.546	13.11	6.483	1.51	0.163	15.8
	200	0.602	15.25	11.17	1.60	0.251	24.1
	225	0.661	17.64	18.09	1.68	0.366	34.7
	250	0.722	20.27	27.84	1.77	0.511	48.0
KCl	40	0.287	3.78	0.060	1.06	0.003	0.34

Table 3 Thermal Conductivities[13]

Salt	Temperature ^{o}C	Solid $k_s \times 10^{2}$, $\frac{W}{cm\text{-}K}$	Saturated Liquid $k_\ell \times 10^{3}$, $\frac{W}{cm\text{-}K}$	Water + Air $k_g \times 10^{4}$, $\frac{W}{cm\text{-}K}$
NaCl	25	5.51	5.81	2.59
	50	5.01	6.11	2.72
	75	4.57	6.33	2.81
	100	4.20	6.47	2.88
	125	3.87	6.53	2.96
	150	3.58	6.52	3.09
	175	3.33	6.45	3.30
	200	3.12	6.31	3.58
	225	2.93	6.12	3.93
	250	2.76	5.85	4.36
KCl	40	5.99	5.81	2.67

Table 4 Transport Parameters[13]

Salt	Temperature ^{o}C	Heat of Vaporization ΔH_v, $\frac{kJ}{mole}$	Salt Diffusivity In Water $D_\ell \times 10^5$, $\frac{cm^2}{sec}$	Soret Coefficient $\sigma \times 10^3$, $\frac{1}{K}$	Concentration effect on Boiling Point Elevation $\frac{\partial \Delta T}{\partial C_s} \times 10^3$, $\frac{K\text{-}cm^3}{mole}$	Temperature effect on salt solubility $\frac{dC_s^{sat}}{dT} \times 10^6$, $\frac{mole}{cm^3\text{-}K}$
NaCl	25	44.29	1.66	-2	1.56	1.58
	50	43.29	2.65	-2	1.77	2.11
	75	42.30	4.00	-2	2.00	2.97
	100	41.29	5.77	-2	2.26	3.40
	125	40.25	8.05	-2	2.53	4.15
	150	39.19	10.90	-2	2.82	4.95
	175	38.10	14.42	-2	3.13	5.78
	200	36.96	18.69	-2	3.44	6.67
	225	35.80	23.85	-2	3.78	7.62
	250	34.60	30.01	-2	4.19	8.68
KCl	40	43.69	3.13	-1.8	1.14	25.2

FIGURE CAPTIONS

Figure 1 Cubical Gas-Liquid Inclusion

Figure 2 Flow in the Liquid Shell

Figure 3 Temperature Gradient in Bubble

Figure 4 Diagram for Calculating the Inclusion Velocity

Figure 5 Migration of Two-Phase Inclusions in NaCl (25^{o} - 250^{o}C)

Figure 6 Migration of Two-Phase Inclusions in KCl (40 ^{o}C)

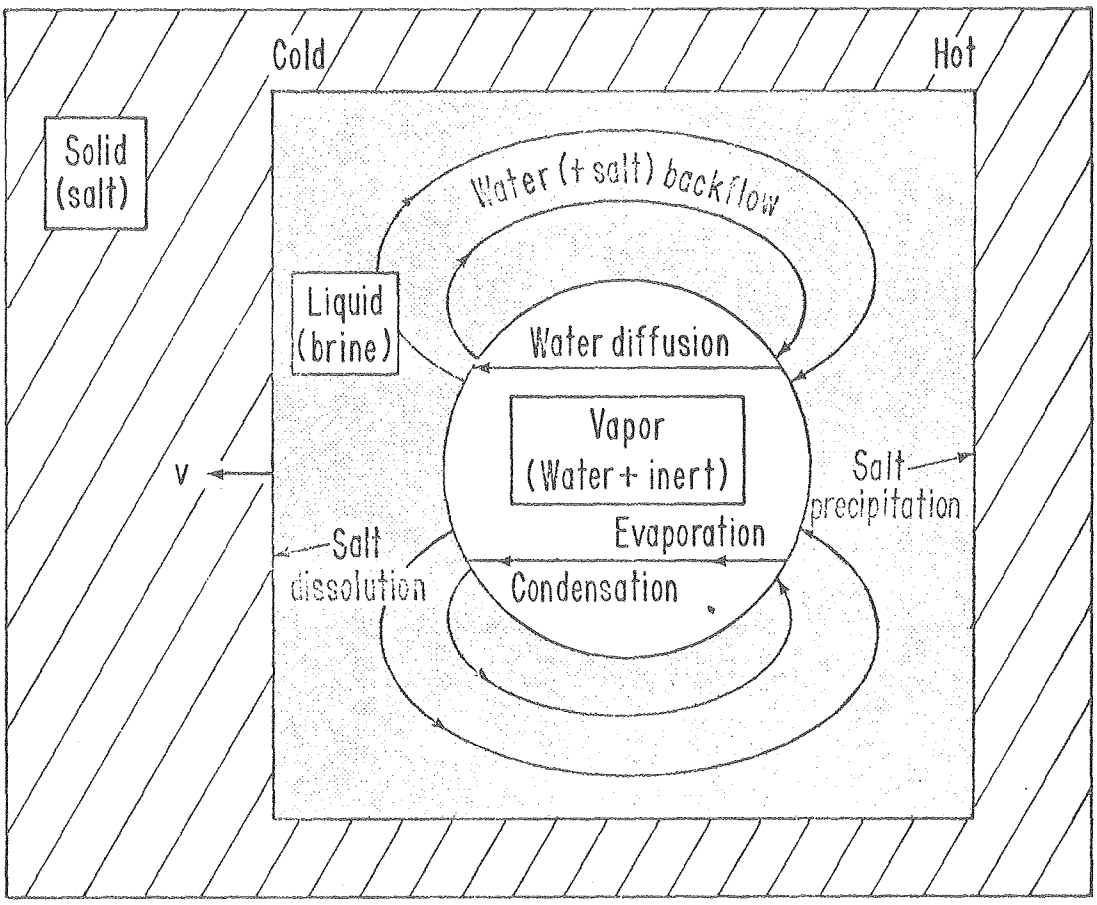

XBL 791-261

FIGURE 1

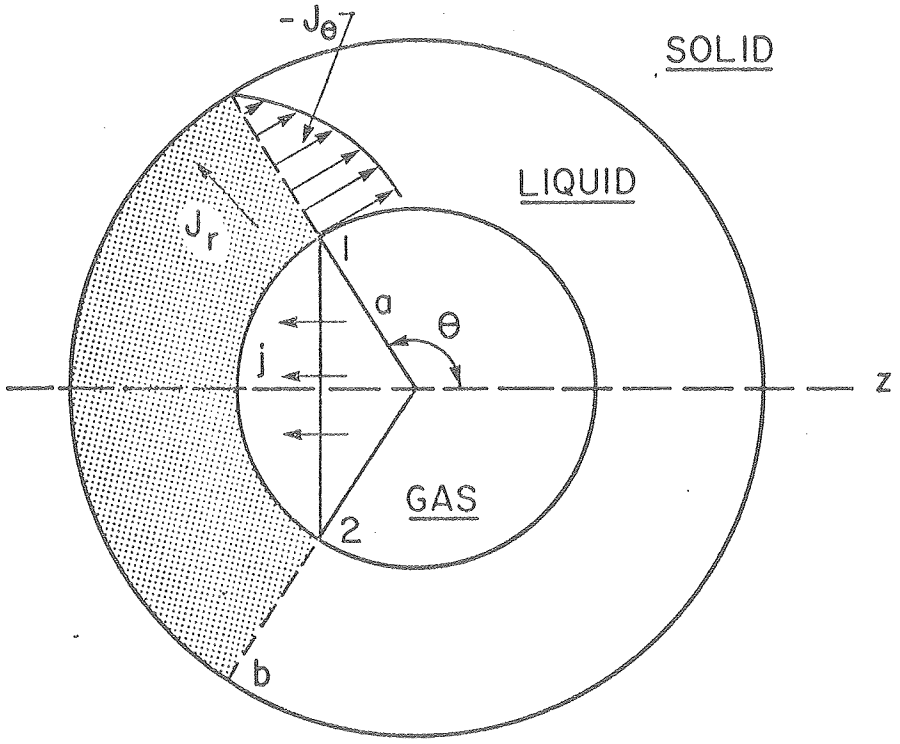

FIGURE 2

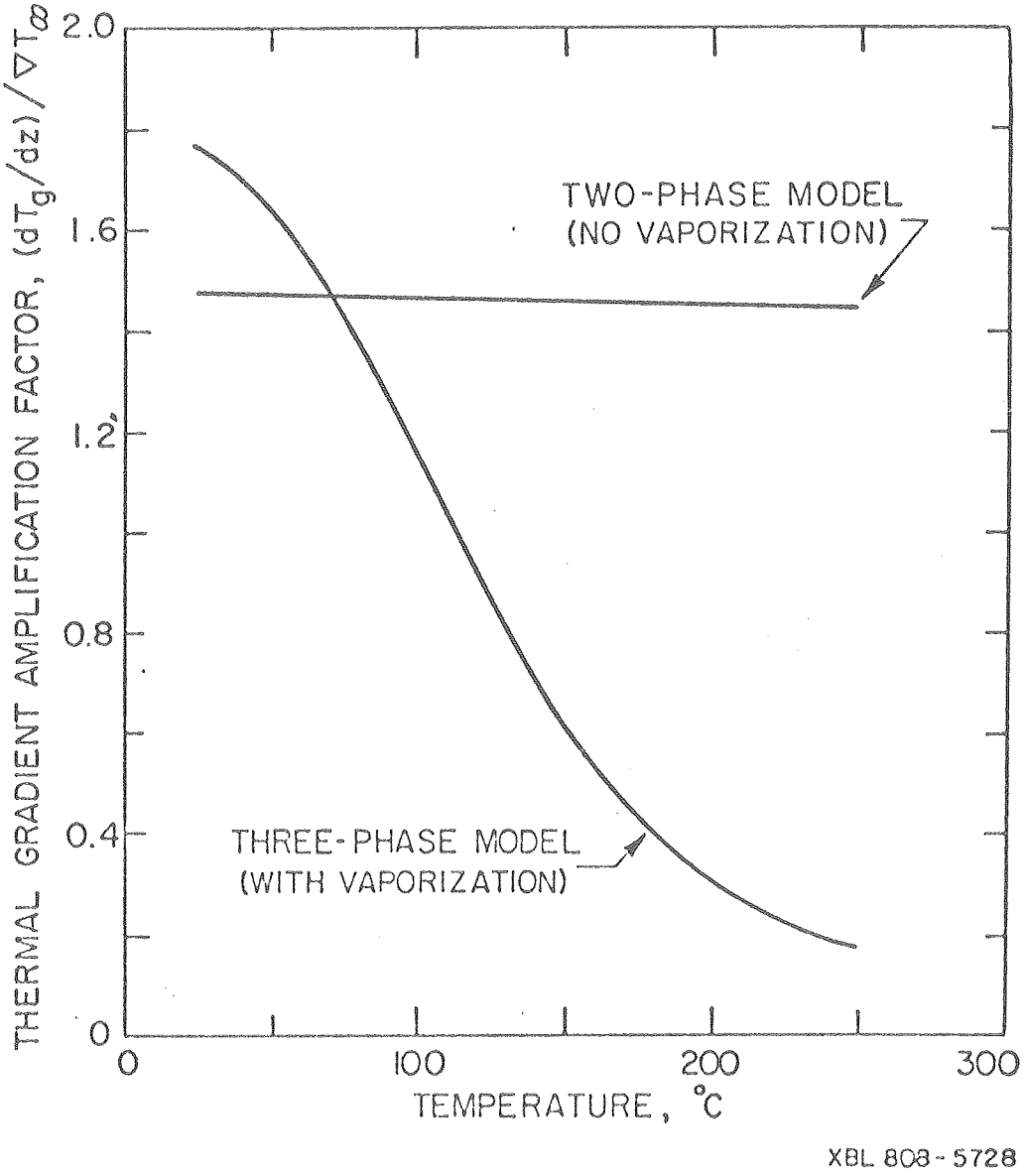
THERMAL GRADIENT AMPLIFICATION FACTOR, $(dT_g/dz)/\nabla T_\infty$
2.0
1.6
1.2
0.8
0.4
0
0
100
200
300
TEMPERATURE, °C
TWO-PHASE MODEL
(NO VAPORIZATION)
THREE-PHASE MODEL
(WITH VAPORIZATION)
XBL 808-5728

FIGURE 3

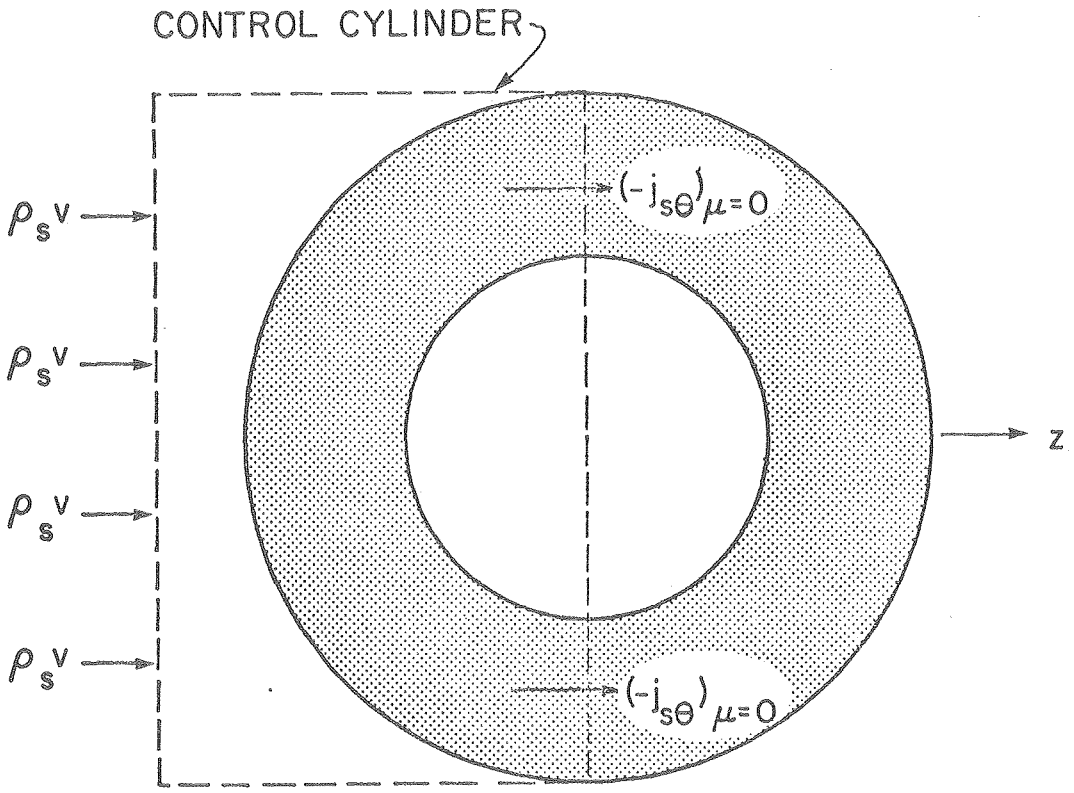
CONTROL CYLINDER
$\rho_s v$
$\rho_s v$
$\rho_s v$
$\rho_s v$
$(-j_{s\theta})_{\mu=0}$
$(-j_{s\theta})_{\mu=0}$
z

FIGURE 4

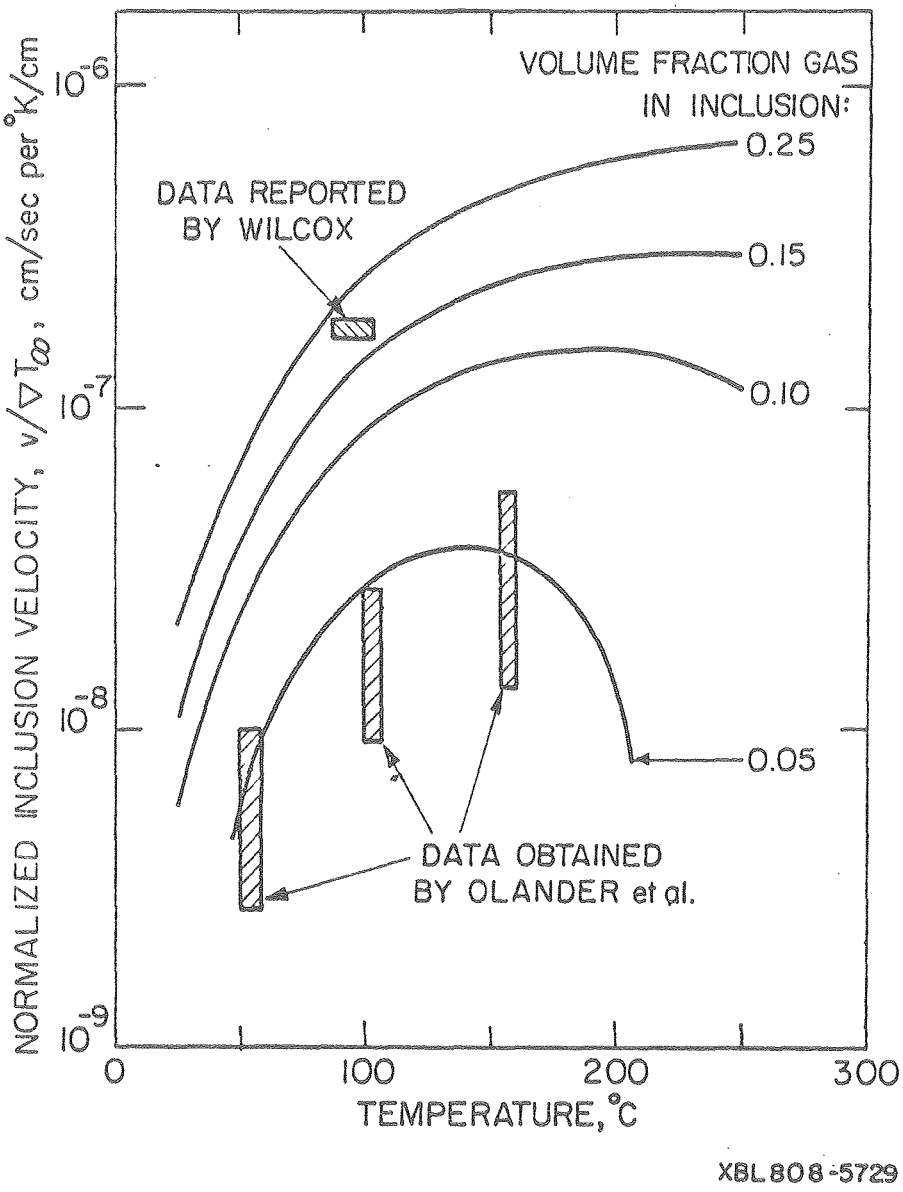
VOLUME FRACTION GAS
IN INCLUSION:
0.25
0.15
0.10
0.05
DATA REPORTED
BY WILCOX
DATA OBTAINED
BY OLANDER et al.
NORMALIZED INCLUSION VELOCITY, $v/\nabla T_\infty$, cm/sec per °K/cm
10^{-6}
10^{-7}
10^{-8}
10^{-9}
0
100
200
300
TEMPERATURE, °C
XBL 808-5729

FIGURE 5

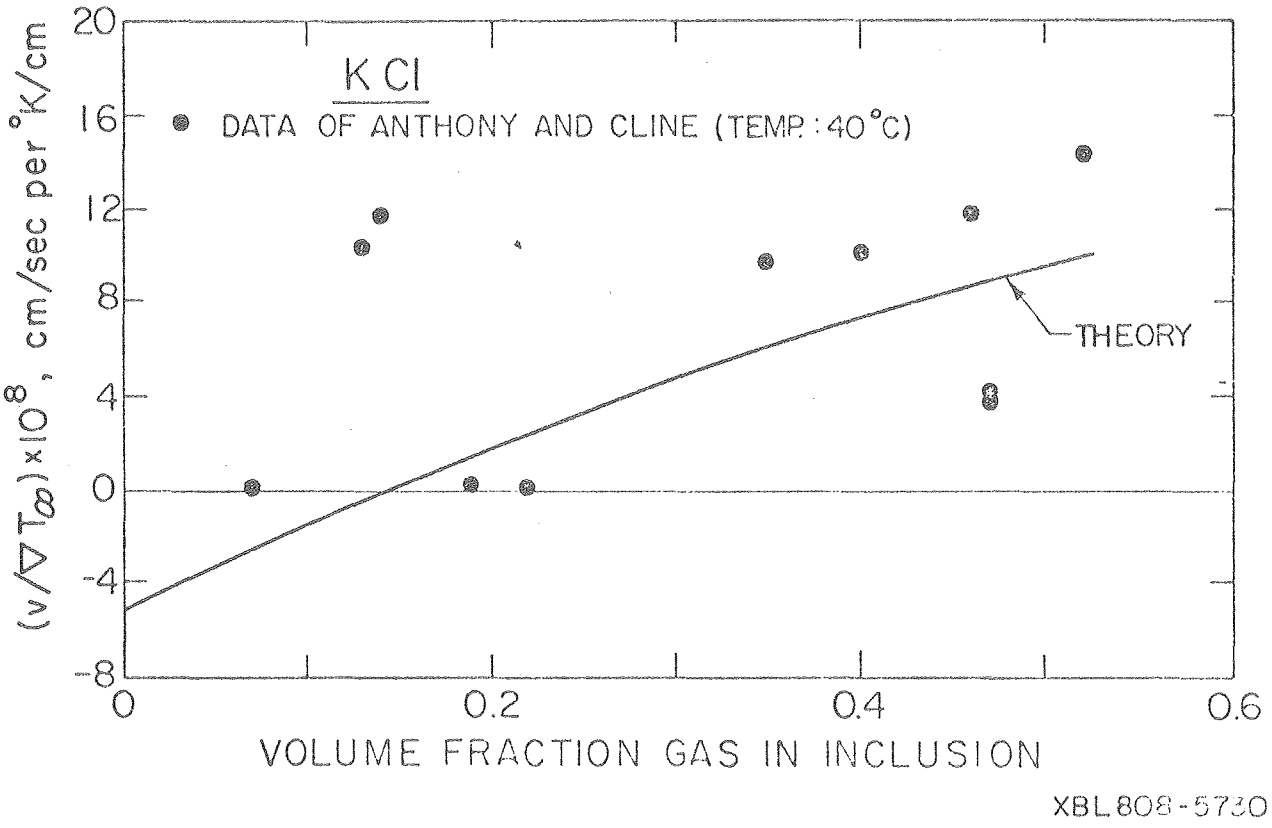
KCl
DATA OF ANTHONY AND CLINE (TEMP.: 40°C)
THEORY
$(v/\nabla T_\infty) \times 10^8$, cm/sec per °K/cm
VOLUME FRACTION GAS IN INCLUSION
20
16
12
8
4
0
-4
-8
0
0.2
0.4
0.6
XBL808-5730

FIGURE 6